AGU PUBLICATIONS

Geophysical Research Letters

RESEARCH LETTER
10.1002/2013GL058172

Key Points:
- Greenland ice sheet surface mass balance variability will grow in the future
- Increased variability is driven by anthropogenic climate forcing
- Increased variability is mainly driven by ablation area growth

Supporting Information:
- Readme
- Comparison of CESM SMB to in situ observations.
- Comparison of CESM SMB mass anomaly seasonal cycle to GRACE seasonal cycle.
- Comparison of CESM SMB to RACMO2 SMB.
- Distribution of Greenland ice sheet surface zones used in study.
- Time series of specific SMB for the constant accumulation and constant ablation zones.
- Series of energy balance components, over Greenland ablation zone.
- Daily progression of melt processes, for present day and end of 21st century.
- Ratio of ablation area to accumulation area-specific SMB variability.
- Ratio of runoff-to-accumulation variability.
- Time series of simple sensitivity simulation which separates role of increased specific sSMB variability and increased ablation zone area, to the overall increase in GIS SMB variability.

Correspondence to:
Jeremy G. Fyke,
fyke@lanl.gov

Citation:
Fyke, J. G., M. Vizcaíno, W. Lipscomb, and S. Price (2014), Future climate warming increases Greenland ice sheet surface mass balance variability, *Geophys. Res. Lett.*, *41*, doi:10.1002/2013GL058172.

Received 7 OCT 2013
Accepted 19 DEC 2013
Accepted article online 26 DEC 2013

Future climate warming increases Greenland ice sheet surface mass balance variability

Jeremy G. Fyke[1], Miren Vizcaíno[2], William Lipscomb[1], and Stephen Price[1]

[1]Los Alamos National Laboratory, Los Alamos, New Mexico, USA, [2]Department of Geoscience and Remote Sensing, Delft University of Technology, Delft, Netherlands

Abstract The integrated surface mass balance (SMB) of the Greenland ice sheet (GrIS) has large interannual variability. Long-term future changes to this variability will affect GrIS dynamics, freshwater fluxes, regional oceanography, and detection of changes in ice volume trends. Here we analyze a simulated 1850–2100 GrIS SMB time series from the Community Earth System Model, currently the only global climate model that realistically simulates GrIS SMB. We find a significant increase in interannual integrated SMB variability over time, which we attribute primarily to a shift to a high-variability melt-dominated SMB regime due to GrIS ablation area growth. We find temporal increases to characteristic ablation and accumulation area-specific SMB variabilities to be of secondary importance. Since ablation area SMB variability is driven largely by variability in summer surface melt, variability in the climate processes regulating the energy fluxes that control melting will likely increasingly determine future GrIS SMB variability.

1. Introduction

The Greenland ice sheet (GrIS) is one of the Earth's two major ice sheets and is currently losing mass [*Shepherd et al.*, 2012; *Hanna et al.*, 2013] with mass loss partitioned roughly equally between decreases in the integrated surface mass balance (iSMB, the difference between integrated accumulation and surface ablation) and increases in discharge from glacier acceleration [*Broecke et al.*, 2009]. Multiple models project a large decline in iSMB to negative values by the end of the 21st century in response to anthropogenic forcing, implying eventual loss of the ice sheet [*Vizcaino et al.*, 2014; *van Angelen et al.*, 2013a; *Fettweis et al.*, 2013]. Superimposed on observed iSMB trends is large interannual iSMB variability [*Box et al.*, 2006, 2012; *Hanna et al.*, 2008], including extreme events such as the 1998, 2007, 2010, and 2012 SMB minima [*Mernild and Liston*, 2012; *van Angelen et al.*, 2013b; *Tedesco et al.*, 2013]. This variability is important for several reasons. First, it affects ice dynamics via the impact of supraglacial melt on basal sliding [*Schoof*, 2010] and via the effects of subglacial freshwater discharge on fjord circulation and outlet glacier melting [*Sciascia et al.*, 2013]. Second, on a larger scale, iSMB variability contributes to variability in the GrIS-sourced freshwater flux to the ocean [*Bamber et al.*, 2012], which could alter local and regional patterns of ocean circulation [*Marsh et al.*, 2010; *Fichefet et al.*, 2003] and long-term sea level trends. Lastly, increases in iSMB variability limit the ability to detect changes in GrIS volume trends [*Wouters et al.*, 2013].

These factors highlight the need to better understand historical and future trends in interannual GrIS iSMB variability. To date, studies have mainly provided time-invariant variability estimates for the recent historical period [e.g., [*Box et al.*, 2006; *Ettema et al.*, 2009; *Vizcaino et al.*, 2013; *van Angelen et al.*, 2013b]. We build on these studies by (a) analyzing time-varying interannual GrIS iSMB variability trends ("interannual" is implied hereafter) generated by a coupled Community Earth System Model (CESM) simulation spanning 1850–2100 under historical and Representative Concentration Pathway 8.5 (RCP8.5) forcing [*van Vuuren et al.*, 2011] and (b) clearly identifying the physical processes controlling the simulated variability changes that we find.

2. Methods

CESM [*Hurrell et al.*, 2013] includes the Community Atmosphere Model and Community Land Model (CLM) at 0.9° × 1.25° resolution and the Parallel Ocean Program and Community Ice Code ocean/sea ice models at 1° resolution. It explicitly resolves Arctic interannual climate variability [*de Boer et al.*, 2012]. Uniquely among global climate models, the CESM also includes non-bias-corrected energy balance-based calculations of GrIS SMB [*Lipscomb et al.*, 2013], which account for detailed snow/ice surface processes such as albedo evolution, snow compaction, and refreezing [*Flanner et al.*, 2007]. SMB calculations are carried out within CLM

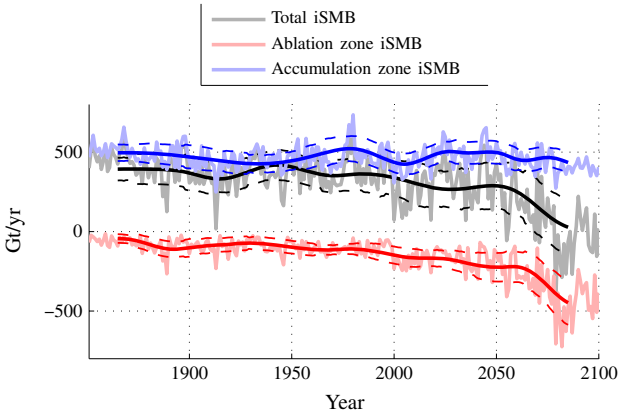

Figure 1. Total iSMB time series (black) and component ablation/accumulation iSMB time series (red/blue). These and subsequent time series have the first and final 15 years removed, to account for the 31 year moving standard deviation windowing. This and subsequent plots show raw time series (faded line), smoothed trends (solid line, generated using empirical mode decomposition, supporting information) and ± 1 standard deviation (dashed lines).

over multiple elevation classes, and the resulting SMB is remapped to present-day GrIS geometry at 5 km resolution [*Bamber et al.*, 2001]. This technique (detailed in the supporting information and *Lipscomb et al.* [2013]) allows for explicit resolution of the currently narrow GrIS ablation area within a global model simulation. CESM-simulated SMB has been comprehensively validated by *Vizcaino et al.* [2013] against 475 in situ observations [*Cogley*, 2004; *Bales et al.*, 2009; *Ettema et al.*, 2009; *van de Wal et al.*, 2012], Gravity Recovery and Climate Experiment data [*Velicogna*, 2009], and relative to SMB calculated by the high-resolution 11 km Regional Atmospheric Climate Model 2 (RACMO2) regional climate model [*van Angelen et al.*, 2013b]. These comparisons (detailed further in Figures S1–S3 in the supporting information and *Vizcaino et al.* [2013]) clearly highlight that CESM realistically simulates recent historical GrIS SMB in terms of magnitude, spatial distribution, and (importantly for this study) historical variability. The success of the CESM in accurately capturing the present state of GrIS SMB, along with its ability to simulate multicentury anthropogenically driven climate trends, makes CESM uniquely well suited to analysis of long-term iSMB variability changes.

The simulation we analyze here was initialized from a multicentury preindustrial CESM control run, followed by a 100 year preindustrial spin-up with SMB calculations enabled. From this steady state, the model was integrated forward under historical forcing from 1850 to 2005 and RCP8.5 forcing from 2006 to 2100. RCP8.5 is currently the most extreme Intergovernmental Panel on Climate Change forcing scenario and results in net radiative forcing of 8.5 W/m^2 by 2100. Under this forcing scenario, we analyze the variability in SMB and its components (snowfall and runoff). We define that variability at year t as 1 standard deviation (σ) of the detrended time series over a 31 year window centered on t. Detrending was carried out using empirical mode decomposition (supporting information). To exclude spurious initial and final variability values and to minimize aliasing, we calculate preindustrial, present and future variability from 31 year averages of annual variability values for the periods 1865–1895, 1970–2000, and 2055–2085.

3. Results

Simulated 1865–1895 GrIS iSMB variability was 90 Gt/yr (Figure 1). For the 1970–2000 period, variability increased to 112 Gt/yr, and for the 2055–2085 period iSMB variability grew to 165 Gt/yr, an increase of 84% relative to 1865–1895 (48% relative to 1970–2000). Both changes are significant at the 99% significance level. The frequency of years exceeding present-day iSMB variability bounds increased by 220% between 1970–2000 and 2055–2085, relative to the moving climatological iSMB mean. Thus, we project that an anthropogenically driven iSMB decline over the 21st century will be accompanied by a significant increase in iSMB variability. The present-day CESM-simulated variability agrees well with the variability simulated by a reanalysis-forced RACMO2 simulation (121 Gt/yr during 1992–2011) [*van Angelen et al.*, 2013b]. In addition, *van Angelen et al.* [2013a] indicate that RACMO2 forced by RCP4.5 HadGEM2-ES output captures a strong future iSMB variability increase (+35 Gt/yr between 1992–2011 and 2079–2098), providing independent

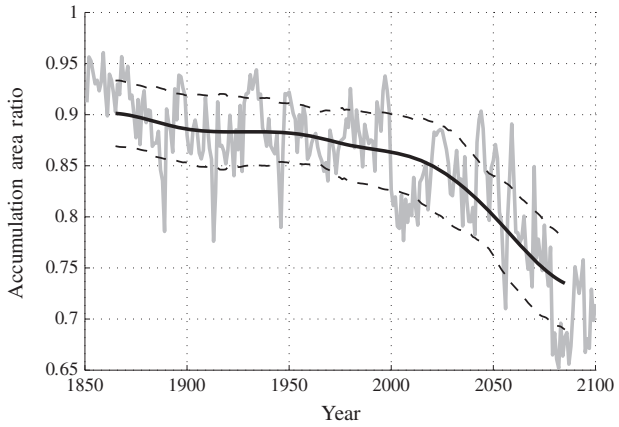

Figure 2. Evolution of the accumulation area ratio (AAR), the ratio of the size of the accumulation area to the total ice sheet area.

corroboration of increased iSMB variability under climate warming. However, *van Angelen et al.* [2013a] do not elaborate on mechanisms behind the RACMO2 variability increase.

To explore the physical mechanism(s) behind increased GrIS iSMB variability, the overall iSMB time series was separated into contributions from the ablation and accumulation areas (Figure 1). The size of these areas covary in extent in response to short-term climate variability and longer-term trends (Figure 2). The preindustrial overall iSMB correlated most highly with accumulation area iSMB ($r = 0.90$ between 1850 and 1880). By 2070–2100, however, the ablation area had emerged as the dominant control on overall iSMB ($r = 0.96$), indicating a long-term shift to an iSMB variability regime dominated by ablation area processes. Furthermore, it is clear that a dramatic 180% increase in ablation area iSMB variability between 1865–1895 and 2055–2085 is the primary cause for the increase in total iSMB variability, when compared to the modest 13% accumulation area iSMB variability increase over the same period.

To explain the overall iSMB variability increase, we first tested the hypothesis that a combination of increases in characteristic ablation area and accumulation area-specific surface mass balance (sSMB, the local vertical SMB flux, units meter per year water equivalent, w.e.) variabilities alone could be responsible for the overall iSMB variability change. To isolate these variabilities, grid cells undergoing exclusively ablation or accumulation for the entire simulation were gathered in separate "ablation-only" and "accumulation-only" bins from which mean sSMB variability trends were extracted (Figures S4 and S5). The mean sSMB in the accumulation-only area increased from 0.31 to 0.37 m/yr w.e. between 1865–1895 and 2055–2085, and the corresponding spatial mean *variability* increased from 0.06 to 0.08 m/yr w.e. (28%). These increases were related to increases in interior mean snowfall and snowfall variability, respectively. In contrast, the mean ablation-only area sSMB decreased from −1.1 m/yr w.e. to −2.4 m/yr w.e., and the corresponding *variability* increased from 0.41 to 0.52 m/yr w.e. (28%). This increased variability was not caused by increased variability of the net summertime ablation-only area surface energy balance components (Figure S6), but rather by a lengthening of the ablation area bare ice season (Figure S7). This increases the dependence of ablation area sSMB variability on summer shortwave radiation variability by lengthening the exposure time of low-albedo glacial ice (which also contributed to a GrIS-wide July albedo decrease of 0.03 over the 21st century [*Vizcaino et al.*, 2014]).

The 28% increases in characteristic accumulation-only and ablation-only sSMB variabilities are notable and reflect the impact of climate change on GrIS snowfall and melting processes, respectively. However, these changes alone cannot quantitatively explain the much larger 84% increase in overall iSMB variability. For this reason, we turn to our second hypothesis, that growth of the high-variability ablation area is behind the overall increase in iSMB variability. Ablation area sSMB variability is substantially higher than accumulation area sSMB variability, with the area mean ratio ($R_{\mathrm{abl:acc}}$) between constant ablation and constant accumulation area sSMB variabilities ranging from 6.5 to 11.5 (with a time mean 8.9, Figure S8). This high $R_{\mathrm{abl:acc}}$ is also found in observational time series of SMB at representative locations [*Van de Wal et al.*, 2005; *van der Veen and Bolzan*, 1999] and in RACMO2 model simulations [*Ettema et al.*, 2009] (supporting information) and arises from a high ratio between the variability of the primary sSMB components in the ablation-only

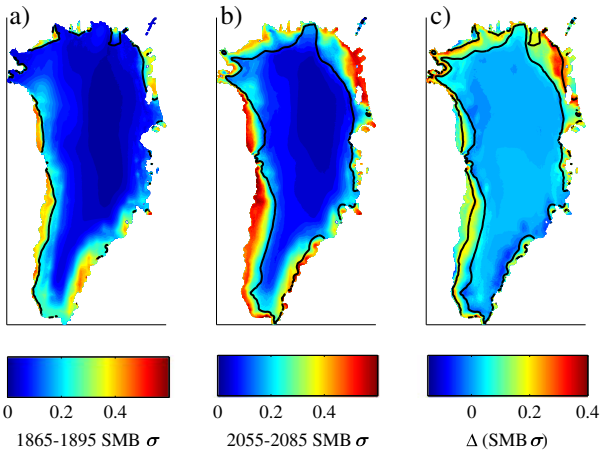

Figure 3. Spatial distribution of sSMB variability (meters per year water equivalent) for (a) 1865–1895, (b) 2055–2085, and (c) the difference in variability between the two periods. Also shown are preindustrial and final climatological ELAs (the line separating the accumulation and ablation areas) for 1850–1880 (Figure 3a), 2070–2100 (Figure 3b), and both (Figure 3c).

and accumulation-only areas: meltwater runoff and snowfall, respectively (10.4, Figure S9). The contrast in sSMB variabilities and the sSMB gradient across the climatological equilibrium line altitude (ELA) are clearly apparent in Figures 3a and 3b.

High ablation area sSMB variability relative to accumulation area sSMB variability suggests that if the ablation area were to expand, the overall GrIS iSMB variability would increase due to a shift from a low-variability accumulation-dominated iSMB regime toward a high-variability, melt-dominated iSMB regime. In support of this reasoning, a 16% decrease in the accumulation area ratio (AAR, the ratio of the accumulation area to the total ice sheet area, Figure 2) is captured by the model as a result of anthropogenically driven climate warming and increased melting [*Vizcaino et al.*, 2014], and Figure 3c highlights that the largest increases in sSMB occur between the 1865–1895 and 2055–2085 ELAs, where accumulation area is transformed to ablation area during the simulation.

To estimate the stand-alone effect of ablation area expansion on overall iSMB variability, we performed two sensitivity experiments. First, ablation area and accumulation area sSMB variabilities were held constant at their initial preindustrial levels, and the AAR was varied according to the trend from the full simulation (supporting information). The long-term 16% decrease in the AAR, with sSMB variabilities held constant, produced a 59% increase in overall iSMB variability between 1850 and 2100. Second, we held the AAR fixed and varied only the sSMB variabilities, which yielded a lower 28% increase in overall iSMB variability. The difference between these two experiments confirms that expansion of the high-variability ablation area is approximately twice as effective as increased sSMB variability in changing iSMB variability and is thus primarily responsible for driving the overall GrIS iSMB variability increase in the coupled CESM simulation.

4. Discussion and Conclusions

We conclude that a significant, anthropogenically forced increase in simulated GrIS iSMB variability between 1850 and 2100 results primarily from ablation area expansion and a resulting shift from an accumulation-dominated to a melt-dominated SMB variability regime. We find simulated stand-alone increases to characteristic ablation and accumulation area sSMB variabilities to be of secondary importance to the overall iSMB increase. In agreement with observations [e.g., *Van de Wal et al.*, 2005], ablation area sSMB variability in CESM is primarily regulated by variability in surface runoff, which is in turn controlled primarily by variability in summer absorbed shortwave radiation. This relationship implies that because of increasing ablation area, future melt-dominated GrIS SMB variability will be increasingly tied to the variabilities of incoming shortwave radiation and surface albedo, which are themselves impacted by regional circulation variability, clouds, and the ice sheet albedo feedback [*Box et al.*, 2012]. In light of the projected shift to a melt-dominated GrIS SMB variability regime, analyses of future changes to these mechanisms is a logical extension of the work presented here, and should be guided by observational studies of GrIS melt variability, including recent melt extremes [e.g., *Hanna et al.*, 2012, 2013; *Bennartz et al.*, 2013]. Better

understanding of the evolving coupling between GrIS summer melt variability and climate is critical, given that this relationship will increasingly control future melt-dominated iSMB variability, with follow-on impacts to ice dynamics, GrIS-sourced ocean freshwater fluxes, ocean circulation, sea level rise, and identification of anthropogenically forced GrIS volume trends.

Acknowledgments
The authors thank William Sacks and Nathan Urban for useful contributions and Editor Julienne Stroeve, reviewer Jan Lenaerts, and another anonymous reviewer for many insightful critiques. This work was supported by the Earth System Modeling and Regional and Global Climate Modeling programs of the Office of Biological and Environmental Research within the U.S. Department of Energy Office of Science.
The Editor thanks Jan Lenaerts and an anonymous reviewer for their assistance in evaluating this paper.

References

Bales, R., Q. Guo, D. Shen, J. McConnell, G. Du, J. Burkhart, V. Spikes, E. Hanna, and J. Cappelen (2009), Annual accumulation for Greenland updated using ice core data developed during 2000–2006 and analysis of daily coastal meteorological data, *J. Geophys. Res.*, *114*, D06116, doi:10.1029/2008JD011208.

Bamber, J., M. van den Broeke, J. Ettema, J. Lenaerts, and E. Rignot (2012), Recent large increases in freshwater fluxes from Greenland into the North Atlantic, *Geophys. Res. Lett.*, *39*, L19501, doi:10.1029/2012GL052552.

Bamber, J. L., R. L. Layberry, and S. Gogineni (2001), A new ice thickness and bed data set for the Greenland ice sheet 1: Measurement, data reduction, and errors, *J. Geophys. Res.*, *106*, 33,773–33,780.

Bennartz, R., M. Shupe, D. Turner, V. Walden, K. Steffen, C. Cox, M. Kulie, N. Miller, and C. Pettersen (2013), July 2012 Greenland melt extent enhanced by low-level liquid clouds, *Nature*, *496*, 83–86, doi:10.1038/nature12002.

Box, J., D. Bromwich, B. Veenhuis, L.-S. Bai, S.-H. Wang, J. Stroeve, T. Haran, J. Rogers, and K. Steffen (2006), Greenland ice sheet surface mass balance variability (1988–2004) from calibrated polar MM5 output, *J. Clim.*, *19*, 2783–2800, doi:10.1175/JCLI3738.1.

Box, J., X. Fettweis, J. Stroeve, M. Tedesco, D. Hall, and K. Steffen (2012), Greenland ice sheet albedo feedback: Thermodynamics and atmospheric drivers, *Cryosphere*, *6*, 821–839, doi:10.5194/tc-6-821-2012.

Cogley, J. (2004), Greenland accumulation: An error model, *J. Geophys. Res.*, *109*, D18101, doi:10.1029/2003JD004449.

de Boer, G., W. Chapman, J. Kay, B. Medeiros, H. Shupe, S. Vavrus, and J. Walsh (2012), A characterization of the present-day Arctic atmosphere in CCSM4, *J. Clim.*, *25*, 2676–2695, doi:10.1175/JCLI-D-11-00228.1.

Ettema, J., M. van den Broeke, E. van Meijgaard, W.J. van de Berg, J. Bamber, J. Box, and R. Bales (2009), Higher surface mass balance of the Greenland ice sheet revealed by high-resolution climate modeling, *Geophys. Res. Lett.*, *36*, L12501, doi:10.1029/2009GL038110.

Fettweis, X., B. Franco, M. Tedesco, J. van Angelen, J. Lenaerts, M. van den Broeke, and H. Gallee (2013), Estimating the Greenland ice sheet surface mass balance contribution to future sea level rise using the regional atmospheric climate model MAR, *Cryosphere*, *7*, 469–489, doi:10.5194/tc-7-469-2013.

Fichefet, T., C. Poncin, H. Goosse, P. Huybrechts, I. Janssens, and H. Le Treut (2003), Implications of changes in freshwater flux from the Greenland ice sheet for the climate of the 21st century, *Geophys. Res. Lett.*, *30*(17), doi:10.1029/2003GL017826.

Flanner, M., C. Zender, J. Randerson, and P. Rasch (2007), Present-day climate forcing and response from black carbon in snow, *J. Geophys. Res.*, *112*, D11202, doi:10.1029/2006JD008003.

Hanna, E., P. Huybrechts, K. Steffen, J. Cappelen, R. Huff, C. Shuman, T. Irvine-Fynn, S. Wise, and M. Griffiths (2008), Increased runoff from melt from the Greenland ice sheet: A response to global warming, *J. Clim.*, *21*, 331–341, doi:10.1175/2007JCLI1964.1.

Hanna, E., J. Jones, J. Cappelen, S. Mernild, L. Wood, K. Steffen, and P. Huybrechts (2012), The influence of North Atlantic atmospheric and oceanic forcing effects on 1900–2010 Greenland summer climate and ice melt/runoff, *Int. J. Climatol.*, *33*, 862–880, doi:10.1002/joc.3475.

Hanna, E., et al. (2013), Ice-sheet mass balance and climate change, *Nature*, *498*, 51–59, doi:10.1038/nature12238.

Hurrell, J. W., et al. (2013), The Community Earth System Model: A framework for collaborative research, *Bull. Am. Meteorol. Soc.*, *94*, 1339–1360, doi:10.1175/BAMS-D-12-00121.

Lipscomb, W., J. Fyke, M. Vizcaíno, W. Sacks, J. Wolfe, M. Vertenstein, T. Craig, E. Kluzek, and D. Lawrence (2013), Implementation and initial evaluation of the Glimmer Community ice sheet Model in the Community Earth System Model, *J. Clim.*, *26*, 7352–7371, doi:10.1175/JCLI-D-12-00557.1.

Marsh, R., D. Desbruyères, J. L. Bamber, B. A. de Cuevas, A. C. Coward, and Y. Aksenov (2010), Short-term impacts of enhanced Greenland freshwater fluxes in an eddy-permitting ocean model, *Ocean Sci.*, *6*(3), 749–760, doi:10.5194/os-6-749-2010.

Mernild, S., and G. Liston (2012), Greenland freshwater runoff. Part II: Distribution and trends, 1960–2010, *J. Clim.*, *25*, 6015–6035, doi:10.1175/JCLI-D-11-00592.1.

Schoof, C. (2010), Ice-sheet acceleration driven by melt supply variability, *Nature*, *468*, 803–806, doi:10.1038/nature09618.

Sciascia, R., F. Straneo, C. Cenedese, and P. Heimbach (2013), Seasonal variability of submarine melt rate and circulation in an East Greenland fjord, *J. Geophys. Res. Oceans*, *118*, 2492–2506, doi:10.1002/jgrc.20142.

Shepherd, A., et al. (2012), A reconciled estimate of ice-sheet mass balance, *Science*, *338*(6111), 1183–1189, doi:10.1126/science.1228102.

Tedesco, M., X. Fettweis, T. Mote, J. Wahr, P. Alexander, J. E. Box, and B. Wouters (2013), Evidence and analysis of 2012 Greenland records from spaceborne observations, a regional climate model and reanalysis data, *Cryosphere*, *7*, 615–630, doi:10.5194/tc-7-615-2013.

van Angelen, J., J. Lenaerts, M. van den Broeke, X. Fettweis, and E. van Meijgaard (2013a), Rapid loss of firn pore space accelerates 21st century Greenland mass loss, *Geophys. Res. Lett.*, *40*, 2109–2113, doi:10.1002/grl.50490.

van Angelen, J., M. Broeke, B. Wouters, and J. Lenaerts (2013b), Contemporary (1960–2012) evolution of the climate and surface mass balance of the Greenland ice sheet, *Surv. Geophys.*, doi:10.1007/s10712-013-9261-z.

Van de Wal, R., W. Greuell, M. den Broeke, C. Reijmer, and J. Oerlemans (2005), Surface mass-balance observations and automatic weather station data along a transect near Kangerlussuaq, West Greenland, *Ann. Glaciol.*, *42*, 311–316, doi:10.3189/172756405781812529.

van de Wal, R. S. W., W. Boot, C. J. P. P. Smeets, H. Snellen, M. R. van den Broeke, and J. Oerlemans (2012), Twenty-one years of mass balance observations along the K-transect, West Greenland, *Earth Syst. Sci. Data*, *4*(1), 31–35, doi:10.5194/essd-4-31-2012.

van den Broeke, M., J. Bamber, J. Ettema, E. Rignot, E. Schrama, W. van de Berg, E. van Meijgaard, I. Velicogna, and B. Wouters (2009), Partitioning recent Greenland mass loss, *Science*, *326*, 984–986, doi:10.1126/science.1178176.

van der Veen, C., and J. Bolzan (1999), Interannual variability in net accumulation on the Greenland ice sheet: Observations and implications for mass balance measurements, *J. Geophys. Res.*, *104*, 2009–2014, doi:10.1029/1998JD200082.

van Vuuren, D., et al. (2011), The representative concentration pathways: An overview, *Clim. Change*, *109*, 5–31, doi:10.1007/s10584-011-0148-z.

Velicogna, I. (2009), Increasing rates of ice mass loss from the Greenland and Antarctic ice sheets revealed by GRACE, *Geophys. Res. Lett.*, *36*, L19503, doi:10.1029/2009GL040222.

Vizcaíno, M., W. Lipscomb, W. Sacks, J. van Angelen, B. Wouters, and M. van den Broeke (2013), Greenland surface mass balance as simulated by the Community Earth System Model. Part I: model evaluation and 1850–2005 results, *J. Clim.*, *26*, 7793–7812, doi:10.1175/JCLI-D-12-00615.1.

Vizcaíno, M., W. Lipscomb, W. Sacks, and M. van den Broeke (2014), Greenland surface mass balance as simulated by the Community Earth System Model. Part II: 21st century changes, *J. Clim.*, *27*(1), 215–226, doi:10.1175/JCLI-D-12-00588.1.

Wouters, B., J. Bamber, M. van den Broeke, J. Lenaerts, and I. Sasgen (2013), Limits in detecting acceleration of ice sheet mass loss due to climate variability, *Nat. Geosci.*, *6*, 613–616, doi:10.1038/NGEO1874.